nature communications

Article

https://doi.org/10.1038/s41467-025-58872-6

Programmable protein stabilization with language model-derived peptide guides

Received: 21 July 2024

Accepted: 2 April 2025

Published online: 15 April 2025

Check for updates

Lauren Hong[1,7], Tianzheng Ye[2,7], Tian Z. Wang[1,7], Divya Srijay[1], Howard Liu[1], Lin Zhao[1], Rio Watson[1], Sophia Vincoff[1], Tianlai Chen[1], Kseniia Kholina[1], Shrey Goel[1], Matthew P. DeLisa[2,3,4] & Pranam Chatterjee[1,5,6]

Dysregulated protein degradation via the ubiquitin-proteasomal pathway can induce numerous disease phenotypes, including cancer, neurodegeneration, and diabetes. While small molecule-based targeted protein degradation (TPD) and targeted protein stabilization (TPS) platforms can address this dysregulation, they rely on structured and stable binding pockets, which do not exist to classically "undruggable" targets. Here, we expand the TPS target space by engineering "deubiquibodies" (duAbs) via fusion of computationally-designed peptide binders to the catalytic domain of the potent OTUB1 deubiquitinase. In human cells, duAbs effectively stabilize exogenous and endogenous proteins in a DUB-dependent manner. Using protein language models to generate target-binding peptides, we engineer duAbs to conformationally diverse target proteins, including key tumor suppressor proteins p53 and WEE1, and heavily-disordered fusion oncoproteins, such as PAX3::FOXO1. We further encapsulate p53-targeting duAbs as mRNA in lipid nanoparticles and demonstrate effective intracellular delivery, p53 stabilization, and apoptosis activation, motivating further in vivo translation.

The ubiquitin-proteasomal pathway regulates critical processes, including protein folding, DNA repair, and cell differentiation, thus helping to maintain proteostasis[1]. Dysregulation of this pathway—such as improper degradation of tumor suppressors or mutant, misfolded proteins—can lead to severe pathogenic phenotypes, such as cancer, neurodegenerative disease, cystic fibrosis, and diabetes[2–5]. Therefore, there is a need for proteome editing tools that are capable of correcting this dysregulation by selectively removing ubiquitin from target proteins. While the controllable installation of ubiquitin has been extensively exploited in the form of targeted protein degradation (TPD) strategies such as PROTACs and molecular glues[1], only recently has the reverse process, targeted protein stabilization (TPS), gained attention[6]. The current state-of-the-art TPS modality, termed deubiquitinase-targeting chimeras or DUBTACs, is analogous to PROTACs: they recruit endogenous deubiquitinases (DUBs), but still rely on the arduous design of chemical linkers and existence of small-molecule warheads, which do not exist for classically "undruggable" proteins due to their conformational disorder and lack of putative or cryptic binding site accessibility[6]. Due to the labor-intensive and time-consuming process of designing de novo binders—whether small molecules or biologics—for target proteins[7], achieving a truly programmable TPS system currently remains unrealized.

In recent years, our team has described a unique TPD strategy that involves genetically fusing target-specific short "guide" peptides, designed via sequence-based algorithms, to the ubiquitin conjugation domain of the human E3 ubiquitin ligase, CHIP[8–12]. Without the requirement of a stable target structure, this programmable design process results in chimeric proteins called "ubiquibodies" (uAbs) for

[1]Department of Biomedical Engineering, Duke University, Durham, NC, USA. [2]Robert F. Smith School of Chemical and Biomolecular Engineering, Cornell University, Ithaca, NY, USA. [3]Nancy E. and Peter C. Meinig School of Biomedical Engineering, Cornell University, Ithaca, NY, USA. [4]Cornell Institute of Biotechnology, Cornell University, Ithaca, NY, USA. [5]Department of Computer Science, Duke University, Durham, NC, USA. [6]Department of Biostatistics and Bioinformatics, Duke University, Durham, NC, USA. [7]These authors contributed equally: Lauren Hong, Tianzheng Ye, Tian Z. Wang.
e-mail: pranam.chatterjee@duke.edu

TPD which can target a conformationally varied array of target proteins[8–12]. Here, we design the analogous platform for TPS, termed deubiquibodies (duAbs), by fusing computationally-designed peptide guides to the catalytic domain of the potent OTUB1 deubiquitinase. Utilizing pre-existing binders, our first-generation fusion duAb architecture effectively stabilizes exogenous and endogenous proteins in a DUB-dependent manner following ectopic expression in human cells. We showcase the inherent programmability of duAbs by swapping in target-binding peptides designed via recent generative protein language models (pLMs), SaLT&PepPr, PepPrCLIP, and PepMLM[10–12]. These peptide-guided duAbs stabilize their intended target substrates, including the transcription factors β-catenin and FOXP3, the tumor suppressors WEE1 and p53, and a disordered fusion oncoprotein PAX3::FOXO1. As a final step toward in vivo translation, we deliver p53-targeting duAbs as mRNA in lipid nanoparticles (LNPs), and demonstrate effective intracellular delivery, p53 stabilization, and apoptosis induction.

Results

Peptide-deubiquitinase catalytic domain fusions stabilize target proteins

Recently, Kanner et al. fused the OTUD1 deubiquitinase domain to yellow fluorescent protein-targeting nanobodies (YFP Nbs) to create enDUBO1 constructs that stabilize target-YFP fusion proteins (Fig. 1A)[13]. We hypothesized that DUB domains exhibiting more potent deubiquitinase activity may improve TPS. To evaluate potential effectors for recruitment, Poirson et al., conducted a proteome-scale induced proximity screen to rank both ubiquitinating and deubiquitinating enzymes in terms of catalytic activity[14]. They isolated a subset of deubiquitinases, including OTUB1 and UCHL1, as well as a SUMOlase, UBC9, with potent stabilization activity (Supplementary Table 1)[14]. Of note, OTUB1 is the endogenous deubiquitinase recruited by DUBTACs (Fig. 1A)[6].

Using known domain annotations of these proteins in UniProt[15], we isolated the catalytic domains of each enzyme and fused them to the aforementioned YFP Nbs via either the GAPGSG linker (used for enDUBO1) termed L1[13] or the flexible GSGSG linker already used in the uAb architecture termed L2 (Supplementary Table 1 and 2). To evaluate these designs, we employed a reporter fusion between the potassium ion channel protein, KCNQ1, and YFP, which was co-transfected in HEK293T cells with KCNQ1's E3 ubiquitin ligase, Nedd4L[13,16]. Our results showed that the YFP Nb-L2-OTUB1 fusion significantly increased KCNQ1-YFP levels, which exceeded the stabilization measured for enDUBO1 (YFP Nb-L1-OTUD1), YFP Nb-L2-UCHL1, and YFP Nb-L2-UBC9. We also sought to determine whether our DUB fusions acted in a DUB-dependent manner by employing the pan-DUB inhibitor PR-619[17]. Importantly, we observed that addition of PR-619 at a standard concentration (4 μM) abrogated stabilization, confirming the DUB-dependent mechanism of these stabilizer constructs (Fig. 1B). To further establish this mechanism, we investigated whether direct OTUB1 catalytic activity affected KCNQ1-YFP stabilization by mutating the catalytic cysteine-91 (C91), as well as the complete OTUB1 catalytic triad with aspartic acid-88 (D88) and histidine-265 (H265)[18,19]..We demonstrate that our OTUB1 C91S and D88A/C91S/H265A (ASA) mutants18 did not yield changes to KCNQ1-YFP expression (Fig. 1C).

We next explored whether the OTUB1 catalytic domain could be guided to target proteins via short peptide binders (Fig. 2A). As first candidates, we chose the β-cat_SnP_7 and β-cat_SnP_8 peptides derived from our SaLT&PepPr algorithm, both of which exhibit nanomolar binding affinity to β-catenin[10]. Our hypothesis was that by fusing these peptides to OTUB1, we would induce stabilization of β-catenin in HEK293T cells, which possess an intact Wnt signaling pathway[20]. We demonstrate that, when fused to β-cat_SnP_7 via L2, the OTUB1 catalytic domain induces statistically significant stabilization of β-catenin-sfGFP proteins and outperformed other DUB fusions (Fig. 2B and Supplementary Fig. 2). We again show that employing the pan-DUB inhibitor PR-619 inhibits DUB-dependent stabilization of β-catenin-sfGFP, as expected. In a similar manner, we exhibit that linking β-cat_SnP_7 to OTUB1 C91S and ASA mutants impedes β-catenin-sfGFP stabilization (Fig. 2C). We additionally demonstrate potent duAb activity within 48–72 h post transfection by monitoring β-catenin-sfGFP expression (Fig. 2D and Supplementary Fig. 4). We corroborated these results by co-transfecting the β-cat_SnP_7-L2-DUB fusions into HEK293T cells alongside TOP-GFP, a fluorescent reporter that serves as a reliable readout of β-catenin–dependent transcriptional activity (Fig. 2E)[21]. Cells transfected with β-cat_SnP_7-L2-OTUB1 exhibited significantly higher Wnt signaling than either untransfected cells or cells transfected with our other DUB fusion candidates (Fig. 2F and Supplementary Fig. 3), and either OTUB1 mutants (Fig. 2G).

Finally, to assess the specificity of our peptide-guided OTUB1 system, we performed one-dimensional liquid chromatography-tandem mass spectrometry (1D-LC-MS/MS) analysis on total proteins harvested from HEK293T cells overexpressing β-catenin-sfGFP, with treatment of either our non-targeting, polyG-L2-OTUB1 fusion or our β-cat_SnP_7-L2-OTUB1 fusion (Fig. 2H and Supplementary Fig. 5). Quantifying the abundances of approximately 9300 proteins, our analysis demonstrated increased levels of both β-catenin-sfGFP and endogenous β-catenin (Fig. 2I, J). In comparison, there were minimal changes in the abundance of other proteins. However, we posit that increased "off-target" protein abundance may likely be attributed to downstream functional changes as a result of β-catenin stabilization. For example, Axin 2 (ACTN2), a known regulator of Wnt signaling[22], was upregulated, as was NEIL1, which initiates colorectal cancer phenotypes by destabilizing DNA damage[23]. Together, these results establish our peptide-guided OTUB1 system, which we henceforth refer to as deubiquibodies or "duAbs", as a potent and accurate system for TPS.

Peptide-generating language models enable programmable target stabilization

Next, we sought to demonstrate duAb programmability by designing peptides to diverse target proteins. As many disease-related proteins are conformationally disordered, we decided to leverage protein language models trained to design peptide binders provided only input sequences, rather than 3D structures (Fig. 3A)[10–12]. We first focused our attention on FOXP3, a classically undruggable transcription factor that plays a central role in the development and function of regulatory T cells (Tregs)[24]. FOXP3 is naturally regulated by the CHIP E3 ubiquitin ligase, which is expressed in HEK293T cells[25]. We applied the SaLT&PepPr interface-prediction algorithm to isolate guide peptides from its well-known interacting partner, NFAT (Supplementary Table 2)[25,26] and subsequently tested the corresponding peptide-guided duAbs in a FOXP3-mCherry HEK293T stable cell line. Our results demonstrate that SaLT&PepPr-derived duAbs induce statistically significant stabilization of FOXP3-mCherry in a DUB-dependent manner, outperforming a duAb composed of a previously-designed P60D2A FOXP3-targeting peptide (Fig. 3B)[27].

Encouraged by the stabilization of FOXP3, we next focused our attention on WEE1, an inhibitor of tumor growth in non-cancerous eukaryotic somatic cells. Specifically, WEE1 acts as a kinase to phosphorylate the cyclin-dependent kinase (CDK1)–cyclin B1 complex[28]. This phosphorylation hinders cell cycle advancement in the S and G2 phases of mitosis[28]. WEE1 has been shown to be regulated by the ubiquitin-proteasomal pathway in hepatocellular carcinoma cell lines and that treatment with a proteasome inhibitor or DUBTAC leads to WEE1 stabilization in these cells[6,29,30]. To target WEE1 for duAb-mediated stabilization, we designed six WEE1-specific peptides via a de novo peptide design algorithm, PepPrCLIP (Supplementary Table 2)[12]. The resulting guide peptides were each fused to OTUB1 in our duAb plasmid and tested in HepG2 hepatocellular carcinoma cells. Immunoblot analysis with an anti-WEE1 antibody revealed that each of

https://doi.org/10.1038/s41467-025-58872-6

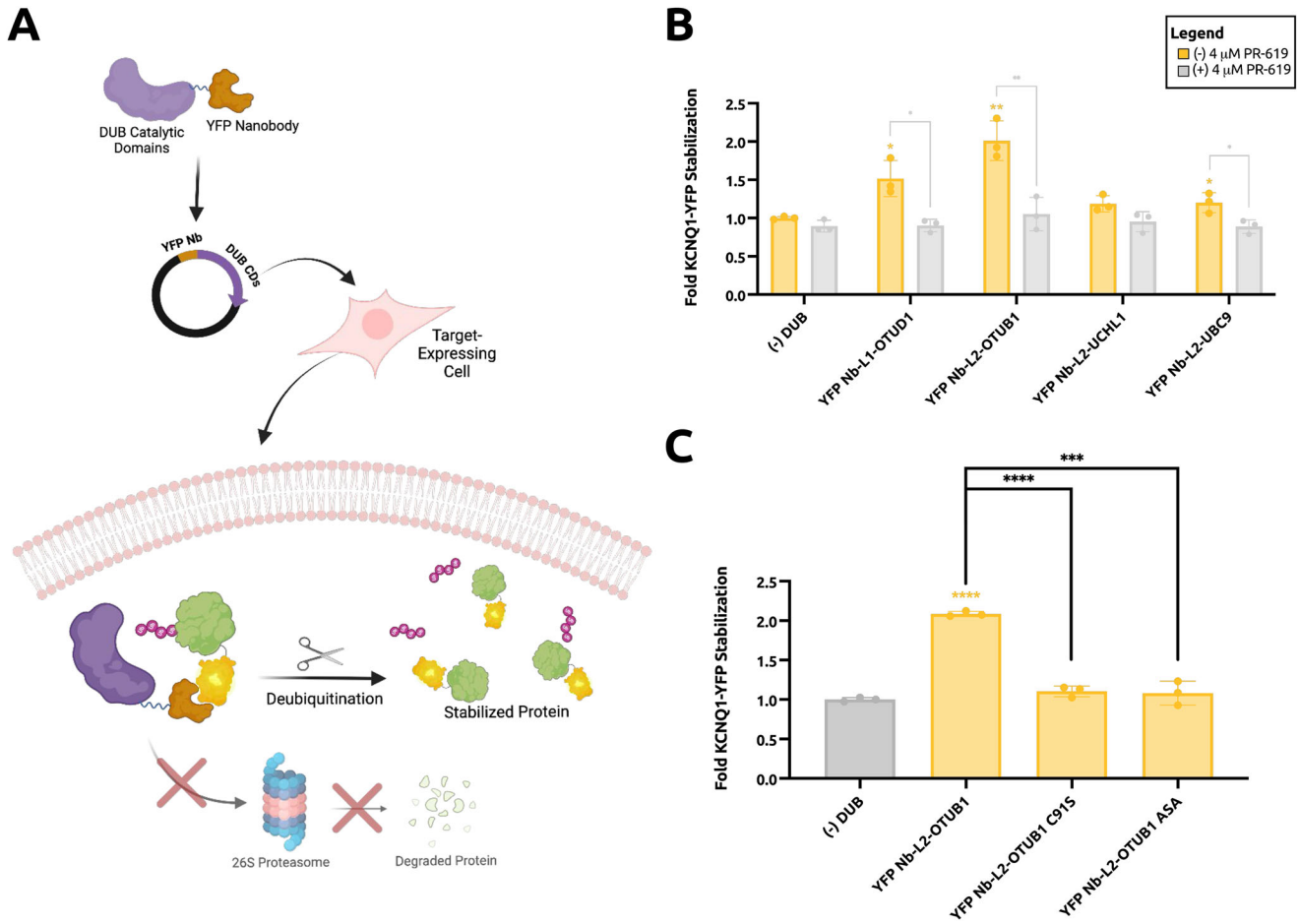

Fig. 1 | Engineering of the duAb architecture. A Building from prior work[13], a YFP nanobody (YFP Nb) was linked to potent deubiquitinase catalytic domains using different linker candidates. Created in BioRender. Hong, L. (2025) https://BioRender.com/v65m595. **B** KCNQ1-YFP stabilization by YFP Nb-based stabilizers in HEK293T cells determined by flow cytometric analysis. Cells were co-transfected with a pcDNA3-Nedd4L vector in the presence or absence of 4 μM PR-619 DUB inhibitor as indicated. Data are the average of independent replicates ($n = 3$). L1 = GAPGSG, L2 = GSGSG. (C) KCNQ-YFP stabilization by YFP Nb-based stabilizers, specifically comparing the YFP Nb-L2-OTUB1 fusion with the OTUB1 C91S and OTUB1 D88A/C91S/H265A (ASA) mutants. Cells were co-transfected with a pcDNA3-Nedd4L vector. Data are the average of individual replicates ($n = 3$). For **B**, **C**, normalized cell fluorescence was calculated by dividing the percentage of YFP + cells in a sample by that of (-) DUB with no DUB inhibitor for control cells. Statistical analysis was performed using the two-tailed Student's *t*-test using GraphPad Prism 10 software, with calculated *p* values are represented as follows: $^{*}p \le 0.05$, $^{**}p \le 0.01$, $^{***}p \le 0.001$, ****, $p \le 0.0001$. Samples with *p* value representations above their respective bars reflect comparisons between the control and that sample; all other *p* value notations compare those specific samples. Please refer to source data for numeric *p* values.

the peptide-guided duAbs induced statistically significant stabilization of endogenous WEE1 (Fig. 3C)[6].

Fusion oncoproteins drive pediatric cancers, such as EWS::FLI1 for Ewing sarcoma, exhibit a "Goldilocks" phenomenon, where suppression of their ubiquitination can induce fusion oncoprotein overdose and cancer cell death[31]. However, pharmacologically stabilizing these proteins is highly difficult, as these proteins exhibit almost complete structural disorder with no discernable binding pockets (Fig. 3D)[32]. To overcome this structural disorder, we used the recently developed peptide generator, PepMLM, which only requires the target sequence as input and outperforms structure-based RFDiffusion[11], to generate ten PAX3::FOXO1-targeting, the predominant driver of pediatric alveolar rhabdomyosarcoma (ARMS)[33]. After transfecting plasmids encoding these peptide-guided duAbs into fusion-positive RH4 ARMS cells, we observed stable increases in the levels of PAX3::FOXO1 fusion oncoprotein for five of the duAb designs (Fig. 3D).

duAbs delivered via lipid nanoparticles induce functional p53 stabilization

Finally, we sought to stabilize p53, a key tumor suppressor protein that regulates cell cycle arrest, apoptosis, and DNA repair in response to cellular stress and DNA damage[34]. The ability to stabilize p53 with duAbs would ensure its availability to suppress tumor formation and growth by maintaining genomic integrity and inhibiting malignant cell proliferation (Fig. 4A)[35]. p53 is largely disordered (Fig. 4B), thus we designed eight peptides using PepMLM[11]. As p53 is destabilized via ubiquitination in human cervical carcinoma, amongst many other cancers, we transfected HeLa cells with plasmid DNA encoding eight different duAb designs[36]. Immunoblot analysis revealed that two duAbs, p53_pMLM_4 and p53_pMLM_5, exhibited potent duAb-dependent stabilization as evidenced by significant increases in endogenous p53 levels (Fig. 4B).

Previous studies have shown successful LNP-mediated delivery of genetically encodable TPD modalities as mRNA[37–41]. Thus, we encapsulated our top p53 stabilizer – p53_pMLM_4-duAb – in LNPs, delivered them in HeLa cells, and showed via immunoblot analysis that we can similarly stabilize endogenous p53 levels (Fig. 4C). We further evaluated downstream functional effects via PARP-1 cleavage, which has been shown to be a hallmark of apoptosis activation (Fig. 4A)[42], and exhibited significant cleaved-PARP-1 expression upon treatment of our p53-stabilizing duAbs (Fig. 4D). In total, these results motivate further in vivo translation of the duAb platform for therapeutic applications.

https://doi.org/10.1038/s41467-025-58872-6

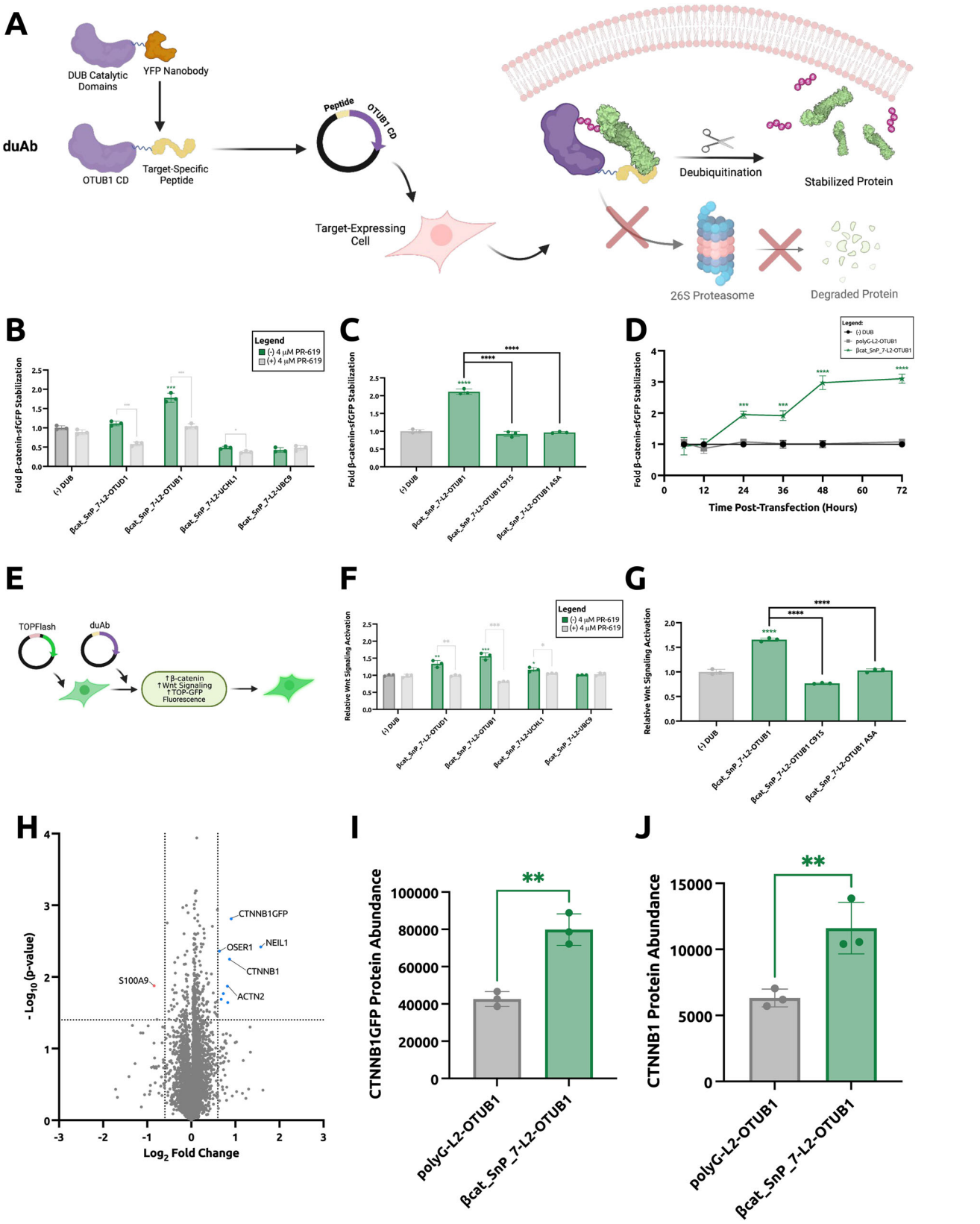

Discussion

In this work, we have demonstrated that our genetically encodable duAbs represent a modular platform for rescuing ubiquitinated proteins, particularly those that are otherwise "undruggable" by conventional small molecule-based strategies. While we see evidence of target stabilization via OTUD1 and OTUB1 domains, we did not observe this same effect for UBC9 and UCHL1. These results can be corroborated with studies that describe UBC9 as a SUMO-conjugating enzyme rather than a hydrolase[43,44]. In comparison, while UCHL1 is a potent deubiquitinase that is well expressed across different cell types, it primarily targets mono-ubiquitinated proteins and binds weakly to poly-ubiquitinated proteins due to the structure of its active site[45,46].

Fig. 2 | Engineering of the duAb architecture using target-specific peptides. **A** Instead of using a YFP Nb, which is not a therapeutically relevant binder, target-specific peptides can instead be leveraged for a more programmable method of protein stabilization. Created in BioRender. Hong, L. (2025) https://BioRender.com/v65m595. **B** β-catenin-sfGFP stabilization in HEK293T cells comparing the four different DUB domain candidates linked to βcat_SnP_7[10] measured by flow cytometric analysis. Cells were transiently transfected in the presence or absence of 4 μM PR-619 DUB inhibitor. Data are the average of independent replicates ($n = 3$). **C** β-catenin-sfGFP stabilization by βcat_SnP_7-linked stabilizers, specifically comparing the βcat_SnP_7-L2-OTUB1 fusion with the OTUB1 C91S and OTUB1 ASA mutants. Data are the average of individual replicates ($n = 3$). **D** Time-course experiment demonstrates that potent duAb activity can be achieved within three days of treatment. Data was collected by extracting treated HEK293T cells at $t = 6$, 12, 24, 36, 48, and 72 h post transfection. **E** TOP-GFP assay for quantifying Wnt signaling in HEK293T cells[21]. Stabilization of endogenous β-catenin results in higher levels of Wnt signaling and increased GFP levels, measured by flow cytometry. Data are the average of independent replicates ($n = 3$). Created in BioRender. Hong, L. (2025) https://BioRender.com/v65m595. **F** TOP-GFP signals in HEK293T cells measured by flow cytometric analysis. Cells were transiently transfected in the presence or absence of 4 μM PR-619 DUB inhibitor. Data are the average of independent replicates ($n = 3$). **G** TOP-GFP signals in HEK293T cells comparing the βcat_SnP_7-L2-OTUB1 fusion with the OTUB1 C91S and OTUB1 ASA mutants measured by flow cytometric analysis. Cells were transiently transfected, and data are the average of independent replicates ($n = 3$). For **B**, **G**, normalized cell fluorescence was calculated by dividing the percentage of sfGFP+ cells in a sample by that of (-) DUB with no DUB inhibitor for control cells. Statistical analysis was performed using the two-tailed Student's *t*-test using GraphPad Prism 10 software, with calculated *p* values are represented as follows: $^{*}p \le 0.05$, $^{**}p \le 0.01$, $^{***}p \le 0.001$, $^{****}p \le 0.0001$. Samples with *p* value representations above their respective bars reflect comparisons between the control and that sample; all other *p* value notations compare those specific samples. **H** Nano LC-MS/MS analysis of total proteins collected from HEK293T cells co-transfected with plasmids encoding β-catenin-sfGFP and either βcat_SnP_7-L2-OTUB1 or polyG-L2-OTUB1. Data was log2-transformed, and a t-test was performed to generate a volcano plot of differentially abundant proteins. Most notably, both exogenous β-catenin-sfGFP (CTNNB1GFP) and endogenous β-catenin (CTNNB1) were among the few proteins that were abundantly present in the β-catenin-stabilizing duAb samples over the non-targeting duAb control. **I** Overexpressed β-catenin-sfGFP (CTNNB1GFP) abundances comparing non-targeting vs. β-catenin-stabilizing duAb treatment in HEK293T cells. **J** Endogenous β-catenin (CTNNB1) abundances comparing non-targeting vs. β-catenin-stabilizing duAb treatment in HEK293T cells. For **I**, **J**, statistical analysis was performed using the one-tailed Student's t-test using GraphPad Prism 10 software, with calculated p values are represented as follows: $^{*}p \le 0.05$, $^{**}p \le 0.01$, $^{***}p \le 0.001$, $^{****}p \le 0.0001$. Please refer to source data for numeric *p* values.

Additionally, while OTUD1's catalytic domain has been leveraged previously[13], its performance was not as strong as the OTUB1 catalytic domain in our study; this may be attributed to its facilitation of K63-deubiquitination rather than K48-deubiquitination, which plays a role in autophagy and pathways other than ubiquitin-proteasome regulation[47,48].

As duAbs are ~290 amino acids in length (Supplementary Table 1), their intracellular delivery, at first glance, poses a challenge for therapeutic application. However, with the rapid advancements of targeted LNP platforms[49], duAbs can be readily encapsulated as mRNA and delivered to specific tissues of interest[37,39], as opposed to DUBTACs, which like PROTACs, may home to any tissue, risking potential side effects and toxicity[50]. Here, we designed LNPs to deliver p53-targeting duAbs, which not only induced p53 stabilization but also activated downstream apoptosis. Interestingly, we noticed that increasing the level of mRNA payload did not increase p53 stabilization efficiency. This may be due to a hook effect, where increasing the amount of payload overdetermined thresholds may lead to lower levels of translated protein[51]. Nonetheless, with further optimization, duAbs delivered via LNPs could provide a targeted and tunable approach for TPS, minimizing off-target effects while maximizing therapeutic efficacy in disease-specific contexts.

Finally, as a genetically encoded tool, peptide-guided duAbs, alongside uAbs, could serve as a powerful platform for proteome-wide target modulation, enabling combinatorial screening of protein activation and inhibition, similar to CRISPRa and CRISPRi for genetic screening[52]. With advances in pLM architectures, our language model-generated peptides can be further optimized to selectively bind post-translational and mutant isoforms of target proteins[53–55], and fused to diverse PTM domains, including kinases, phosphatases, acetylases, and deglycosylases[7]. In total, this study represents a next step towards this eventual goal of a fully programmable proteome editing system.

Methods

Binder design

The β-cat_SnP_7 peptide[10], β-cat_SnP_8 peptide[10], P60D2A peptide[27], and YFP nanobodies[13] were described in previous works and obtained from respective manuscript metadata. Binding peptides designed in this study were either generated by the previously-described SaLT&PepPr algorithm[10] (https://huggingface.co/ubiquitx/saltnpeppr) via input of an interacting partner sequence, by the de novo PepPrCLIP algorithm[12] (https://huggingface.co/ubiquitx/peppprclip) via input of the target protein sequence, or by the target sequence-conditioned PepMLM algorithm[11] (https://huggingface.co/ChatterjeeLab/PepMLM-650M)[11]. All binder sequences can be found in Supplementary Table 2.

Plasmid generation

All duAb plasmids were generated from the standard pcDNA3 vector, harboring a cytomegalovirus (CMV) promoter. An Esp3I restriction site was introduced immediately upstream of the OTUB1 catalytic domain and flexible GSGSG linker via the KLD Enzyme Mix (NEB, Cat # M0554S) following PCR amplification with mutagenic primers (Azenta). For duAb assembly, oligos for candidate peptides were annealed and ligated via T4 DNA Ligase (NEB, Cat # M0202S) into the Esp3I-digested duAb backbone. Assembled constructs were transformed into 50 μL NEB Turbo Competent *Escherichia coli* cells (NEB, Cat # C2984H), and plated onto LB agar supplemented with the appropriate antibiotic for subsequent sequence verification of colonies and plasmid purification (Azenta).

Cell culture

The HEK293T and HeLa cell lines were maintained in Dulbecco's Modified Eagle's Medium (DMEM, Gibco Cat # 11995073) supplemented with 100 units/mL penicillin, 100 mg/mL streptomycin (Gibco, Cat # 15140122), and 10% fetal bovine serum (FBS, Gibco, Cat # A5670402). The hepatocellular carcinoma cell line, HepG2, was maintained in Eagle's Minimum Essential Medium (EMEM, Sigma Aldrich Cat # M2279-500ML) supplemented with 100 units/mL penicillin, 100 mg/mL streptomycin, and 10% fetal bovine serum (FBS). The alveolar rhabdomyosarcoma cell line, RH4, was maintained in RPMI 1640 supplemented with 100 U/mL penicillin, 100 mg/mL streptomycin, and 10% fetal bovine serum (FBS). The RH4 cell line was a generous gift from Dr. Corinne Linardic. For duAb screening in reporter cell lines, pcDNA-duAb (500 ng) plasmids were transfected into cells as triplicates (2×10^5/well in a 24-well plate) with Lipofectamine 2000 (Invitrogen, Cat # 11668027) in Opti-MEM (Gibco, Cat # 31985062). After 2 days post transfection, 4 μM PR-619 (DUB inhibitor, MedChemExpress, Cat # HY-13814) was added to applicable cells (with equivalent volume of media added to non-treated cells), and subsequently cells were harvested within 24 hours post-treatment and analyzed on a Attune NxT Flow Cytometer (ThermoFisher) for GFP fluorescence (488-nm laser excitation, 530/30 filter for detection) and mCherry fluorescence (561-nm laser excitation, 620/15 filter for

https://doi.org/10.1038/s41467-025-58872-6

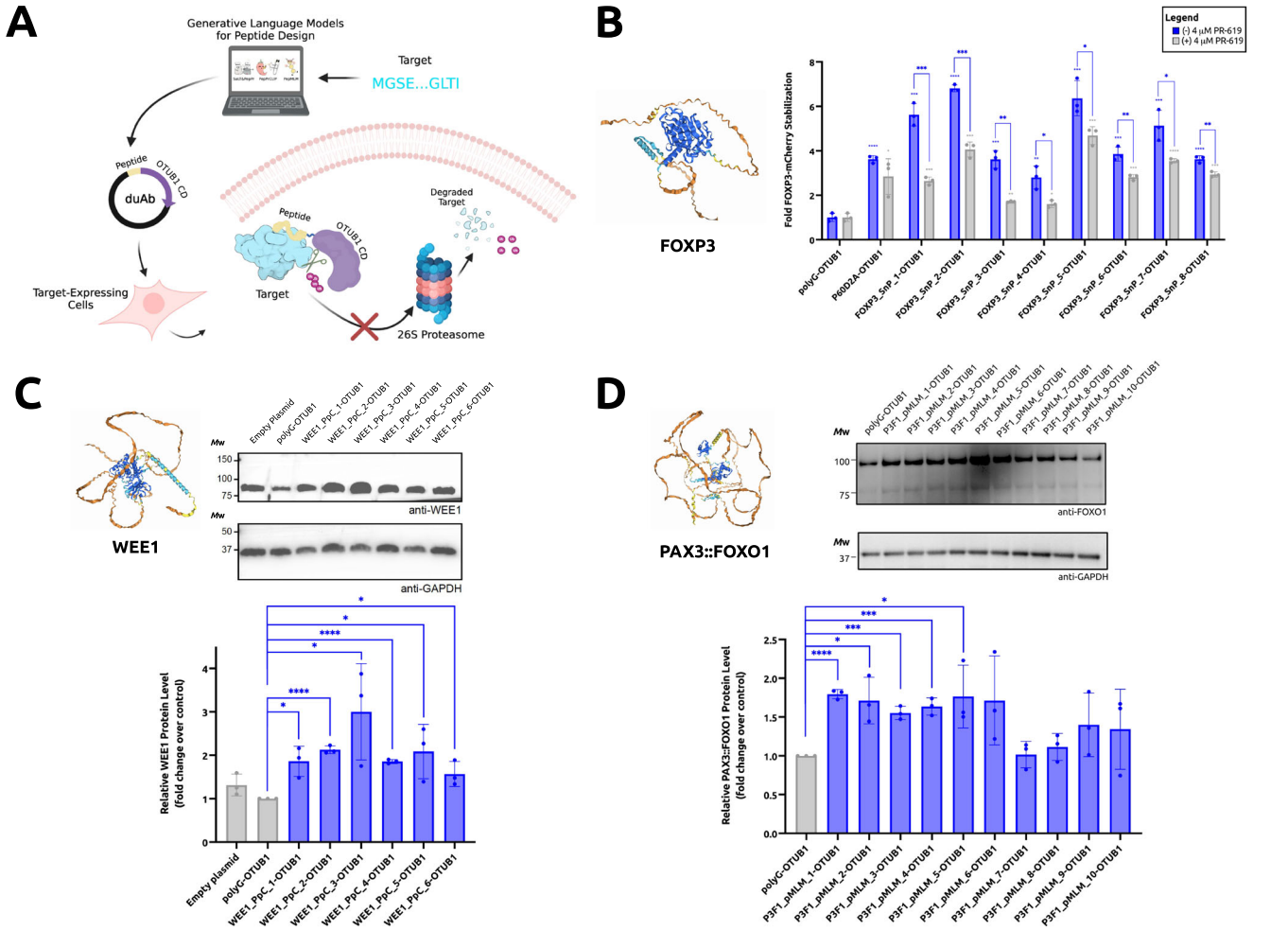

Fig. 3 | Programmable target stabilization via language model-derived peptides. A Programmable target stabilization via language model-derived peptides. Created in BioRender. Chatterjee, P. (2025) https://BioRender.com/h25h541. **B** FOXP3-mCherry stabilization in HEK293T cells. Cellular mCherry fluorescence was measured by flow cytometry in independent replicates ($n = 3$). Normalized cell fluorescence was calculated by dividing the percentage of mCherry+ cells in a sample by that of control cells expressing a duAb vector expressing a non-specific poly-glycine (polyG) control peptide sequence. **C** Stabilization of endogenous WEE1 in protein extracts of HepG2 cells analyzed by immunoblotting. Cells were transiently transfected with a pcDNA3 plasmid encoding a polyG-OTUB1 control or one of the peptide-guided OTUB1 constructs as indicated. Transient transfection with an empty pcDNA3 plasmid served as an additional control. Blots were probed with anti-WEE1 and anti-GAPDH antibodies and are representative of biological replicates ($n = 3$) and technical replicates ($n = 2$) with similar results. **D** Stabilization of endogenous PAX3::FOXO1 in protein extracts of RH4 cells analyzed by immunoblotting. RH4 cells were transiently transfected with a pcDNA3 plasmid encoding one of the candidate duAbs while transfection with a polyG peptide-guided duAb served as a control. Blots were probed with anti-FOXO1 and anti-GAPDH antibodies and are representative of biological replicates ($n = 3$). For all immunoblots in (**C**) and (**D**), an equivalent amount of protein was loaded in each lane. Molecular weight (*M*W) ladder is indicated at left. Intensity of target protein bands was calculated via densitometry and normalized to intensity of GAPDH loading control and then normalized to polyG-OTUB1 control. Data are the average of biological replicates and technical replicates ($n = 3$ for WEE1 and PAX3::FOXO1). Statistical analysis for this figure was performed using the two-tailed Student's *t*-test using GraphPad Prism 10 software, with calculated *p* values are represented as follows: $^{*}p \le 0.05$, $^{**}p \le 0.01$, $^{***}p \le 0.001$, $^{****}p \le 0.0001$. The *p* values above each bar in the fold stabilization and densitometry analyses represent the comparison between the control (polyG-OTUB1, no DUB inhibitor) and the respective sample; all other *p* value notations compare the specified samples. Please refer to source data for numeric *p* values. All structures were predicted via the AlphaFold3 server, and the shading was done according to AlphaFold's confidence metric, plDDT, as follows: Very low (plDDT <50) = Orange, Low (70 > plDDT > 50) = Yellow, Confident (70 > plDDT > 90) = Light Blue, Very high (plDDT > 90) = Light Blue.

detection). 10,000 events were gated for data analysis based on default FSC/SSC parameters for the analyzed cells. Cells expressing eGFP and mCherry were gated, and these were normalized to a sample transfected with a non-targeting duAb using the FlowJo software (https://flowjo.com/). Representative flow cytometry gating strategies are indicated in Supplementary Fig. 1. For endogenous target screening in cell lines, pcDNA-duAb (800 ng) plasmids were transfected into cells as duplicates (3×10^5/well in a 12-well plate) with Lipofectamine 2000 (Invitrogen) in Opti-MEM (Gibco). Cells were harvested after 72 h for subsequent cell fractionation and immunoblotting.

Lentiviral production

For target-reporter packaging, HEK293T cells were seeded in a 6-well plate and transfected at ~50% confluency. For each well, 0.5 µg pMD2.G (Addgene #12259), 1.5 µg psPAX2 (Addgene #12260) and 0.5 µg of the target-mCherry reporter transfer vector were transfected with Lipofectamine 3000 (Invitrogen) according to the manufacturer's protocol. The medium was exchanged 8 hours post transfection, and the viral supernatant was harvested at 48 and 72 hours post transfection. The viral supernatant was concentrated to 100x in 1× DPBS using Lenti-X Concentrator (Clontech, Cat # 631232) according to the manufacturer's instructions, and stored at −80 °C for further use.

https://doi.org/10.1038/s41467-025-58872-6

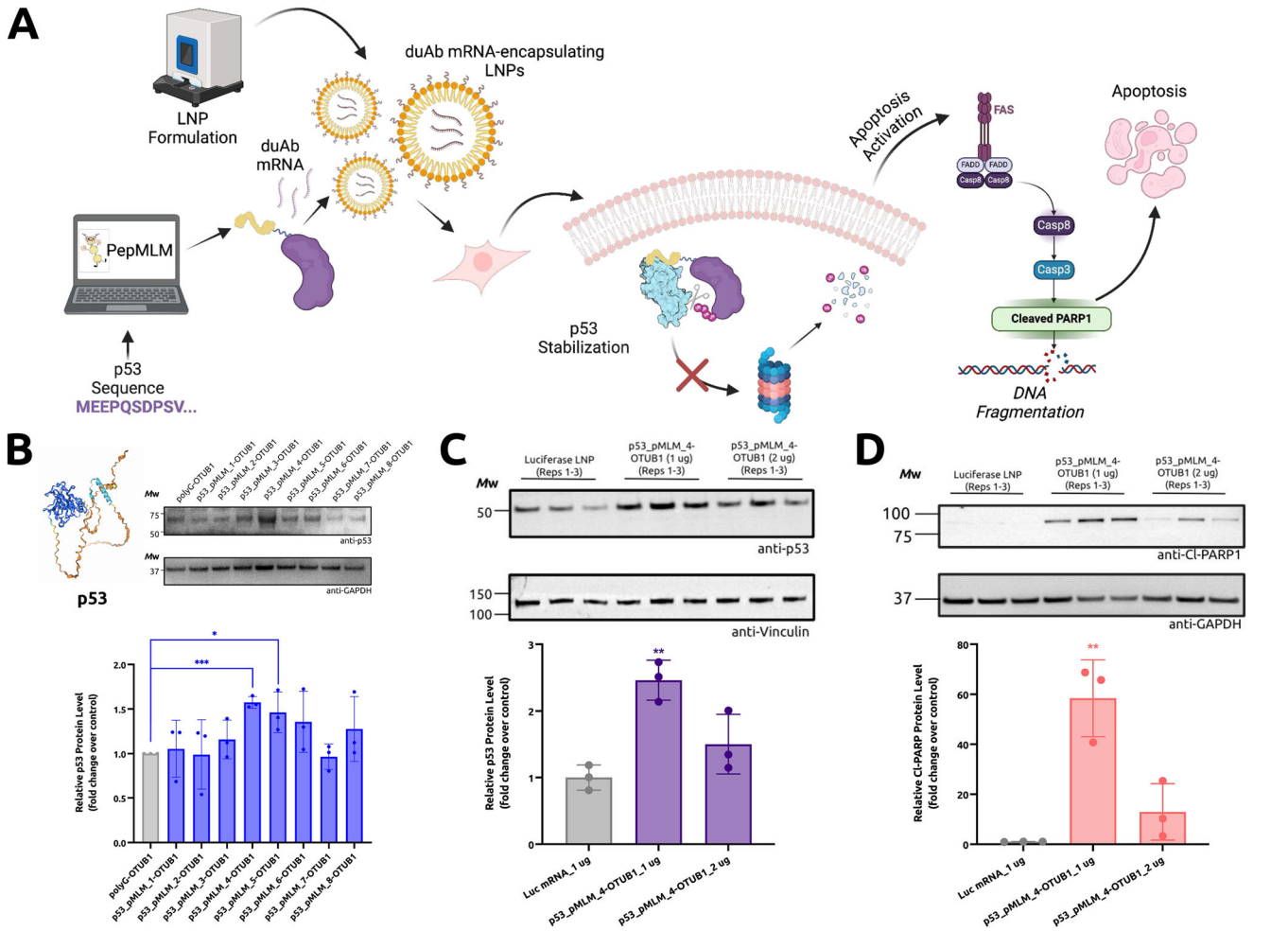

Fig. 4 | Stabilization of p53 and activation of apoptosis via LNPs encapsulating p53-targeting duAbs. A Programmable design of p53-targeting duAbs, encapsulation and delivery via mRNA-encapsulated lipid nanoparticles (LNPs), and downstream apoptosis activation. Created in BioRender. Wang, T. (2025) https://BioRender.com/x61p552. **B** Stabilization of endogenous p53 in protein extracts of HeLa cells analyzed by immunoblotting. HeLa cells were transiently transfected with a pcDNA3 plasmid encoding one of the candidate duAbs while transfection with a polyG peptide-guided duAb served as a control. An equivalent amount of protein was loaded in each lane. Blots were probed with anti-p53 and anti-GAPDH antibodies and are representative of biological replicates ($n = 3$). **C** Stabilization of endogenous p53 in protein extracts of HeLa cells after the best p53-stabilizing duAb (p53_pMLM_4-OTUB1) was delivered via LNPs analyzed by immunoblotting. HeLa cells were transiently transfected with LNPs encapsulating p53_pMLM_4-duAbs encoded as mRNA (loaded 1 µg and 2 µg, respectively) while transfection with luciferase-encoding mRNA-LNP served as a control. An equivalent amount of protein was loaded in each lane. Blots were probed with anti-p53 and anti-Vinculin antibodies and are representative of biological replicates ($n = 3$). **D** Increase in apoptosis hallmark cleaved-PARP-1 (Cl-PARP-1) in protein extracts of HeLa cells after the best p53-stabilizing duAb (p53_pMLM_4-OTUB1) was delivered via LNPs analyzed by immunoblotting. HeLa cells were transiently transfected with LNPs encapsulating p53_pMLM_4-duAbs encoded as mRNA (loaded 1 µg and 2 µg, respectively) while transfection with luciferase-encoding mRNA-LNP served as a control. An equivalent amount of protein was loaded in each lane. Blots were probed with anti-Cl-PARP-1 and anti-Vinculin antibodies and are representative of biological replicates ($n = 3$). For all immunoblots in (**B**–**D**), an equivalent amount of protein was loaded in each lane. Molecular weight (*MW*) ladder is indicated at left. Intensity of target protein bands was calculated via densitometry and normalized to intensity of GAPDH and Vinculin loading controls and then normalized to applicable controls (polyG-OTUB1 for (**B**) and luciferase LNP for (**C**) and (**D**)). Data are the average of biological replicates and technical replicates ($n = 3$ for p53 and Cl-PARP-1). Statistical analysis for this figure was performed using the two-tailed Student's *t*-test using GraphPad Prism 10 software, with calculated *p* values are represented as follows: $^{*}p \le 0.05$, $^{**}p \le 0.01$, $^{***}p \le 0.001$, $^{****}p \le 0.0001$. The *p* values above each bar in the fold stabilization and densitometry analyses represent the comparison between the control (polyG-OTUB1, luciferase LNP) and the respective sample; all other *p* value notations compare the specified samples. Please refer to source data for numeric *p* values. The structure for p53 was predicted via the AlphaFold3 server, and the shading was done according to AlphaFold's confidence metric, plDDT, as follows: very low (plDDT <50) = orange, low (70 > plDDT > 50) = yellow, confident (70 > plDDT > 90) = light blue, very high (plDDT > 90) = light blue.

Target-mCherry reporter monoclonal cell line generation

For target-reporter cell line generation, 1×10^5 HEK293T cells were mixed with 20 µL of the concentrated virus in a 6-well plate. Media was changed 24 h post transduction. Antibiotic selection was started 36 h post transduction by adding 2 µg/mL puromycin (Sigma, Cat # P8833). Cells were harvested for sorting at 5 days post antibiotic selection, and a single cell of mCherry positive was plated in a 96-well plate. Genomic PCR was performed after cell growth to validate the genotype of the monoclonal cell line.

Proteomics

HEK293T cells were maintained in DMEM supplemented with 100 U/mL penicillin, 100 mg/mL streptomycin, and 10% FBS. Target-sfGFP (1 µg) + pcDNA3-duAb (1 µg) plasmids were transfected into cells as triplicates (5×10^5/well in a 6-well plate) with Lipofectamine 2000 (Invitrogen) in Opti-MEM (Gibco). After 72 h post transfection, cells were harvested and washed four times with 500 µL 1× cold PBS. The cell pellets were resuspended in 300 µL Pierce RIPA buffer (ThermoFisher, Cat # 89900) and incubated on ice for 30 min. The

homogenates were treated with 20% (w/v) SDS in triethylammonium bicarbonate buffer, pH 8.5 (Sigma Aldrich, Cat # T7408), followed by probe sonication and heating at 80 °C for 5 min. The supernatants were collected after centrifugation and the concentrations were determined using detergent-compatible Bradford assay. From each sample, 20 µg was reduced and alkylated, and digested with trypsin using an S-trap micro device. Peptide eluents were lyophilized, and after reconstitution, equal volumes of each sample were mixed to make an SPQC pool. Approximately 1 µg of each sample, and three replicates of the SPQC pool were analyzed by 1D-LCMS/MS. Samples were analyzed using a M-Class UPLC system (Waters) coupled to an Exploris 480 high resolution accurate tandem mass spectrometer (ThermoFisher) via a Nanospray Flex Ion source and processed using Spectronaut 16. The p values were calculated by performing a Student's t-test on $\log_2$fc values. The $\log_2$fc values were calculated by the difference of average abundances of the proteins in the presence and absence of targeting duAbs.

Functional assays

For the TOP-GFP assay, 2×10^5 HEK293T cells/well were seeded on a 24-well plate 20–24 h prior to transfection. On the day of transfection, each well received the following plasmids: TOP-GFP plasmid (Addgene #35489) and a duAb plasmid. A total of 500 ng of plasmid DNA in a ratio of TOP-GFP:duAb plasmids = 1:1 was mixed with Lipofectamine 2000 reagent (Invitrogen) in serum-free Opti-MEM medium (Gibco) and added dropwise to each well after incubation at room temperature for 20 min. After 72 h of incubation, cells were harvested and analyzed similarly as mentioned for duAb screening. Viable, single cells were gated, and normalized EGFP cell fluorescence was calculated as compared to a sample transfected with a non-targeting duAb, using the FlowJo software (https://flowjo.com/).

Preparation of lipid nanoparticles encapsulating p53-stabilizing duAbs

mRNA with ARCA cap and poly(A) tail additions for p53_pMLM_4-OTUB1 was synthesized via in vitro transcription using the HiScribe T7 ARCA mRNA Kit (NEB, Cat # E2060S). The mRNA was then concentrated and cleaned of impurities using the RNEasy MinElute Cleanup Kit (Qiagen, Cat # 74204). CleanCap® FLuc mRNA (NEB, Cat # L7602-100) was used as a control. Lipid nanoparticles (LNPs) were prepared by diluting DLIN-MC3-DMA (MedKoo Biosciences, Cat # 555308), DSPC (Avanti Polar Lipids, Cat # 850365P-500mg), Cholesterol (Sigma Aldrich, Cat # C3045), and DMG-PEG2000 (NOF American Corporation, Cat # GM-020) in ethanol using standard molar ratios 50:10:38.5:1.5, respectively. The prepared mRNA for p53_pMLM_4-OTUB1 and luciferase were diluted in 10 mM citrate buffer (ThermoFisher, Cat # J61249.AP) in a 2:1 volume ratio with the lipid mixture, and mRNA was loaded in a 1:20 mass ratio with the lipid, respectively, in a NanoAssemblr™ Spark™ nanoparticle formulation system (Cytiva, Cat # NIS0001). After LNP production, they were transfected into HeLa cells 48 h post-seeding and were extracted 72 h post transfection for immunoblot analysis.

Cell fractionation and immunoblotting

On the day of harvest, cells were detached by addition of 0.05% trypsin-EDTA and cell pellets were washed twice with ice-cold 1× PBS. Cells were then lysed and subcellular fractions were isolated from lysates using a 1:100 dilution of protease inhibitor cocktail (Millipore Sigma, Cat # P8340) in Pierce RIPA buffer (ThermoFisher, Cat # 89900). Specifically, the protease inhibitor cocktail-RIPA buffer solution was added to the cell pellet, the mixture was placed at 4 °C for 30 min followed by centrifugation at 15,000 rpm for 10 min at 4 °C. The supernatant was collected immediately to pre-chilled PCR tubes and quantified using the Pierce BCA Protein Assay Kit (ThermoFisher, Cat # 23227). Twenty micrograms lysed protein was mixed with 4× Bolt™ LDS Sample Buffer (ThermoFisher, Cat # NP0007) with 5% β-mercaptoethanol (Millipore Sigma, Cat # M3148) in a 3:1 ratio and subsequently incubated at 95 °C for 10 min prior to immunoblotting, which was performed according to standard protocols. Briefly, samples were loaded at equal volumes into Bolt™ Bis-Tris Plus Mini Protein Gels (ThermoFisher, Cat # NW04125BOX) and separated by electrophoresis. iBlot™ 2 Transfer Stacks (Invitrogen) were used for membrane blot transfer, and following a 1 h room-temperature incubation in 5% milk-TBST, proteins were probed with rabbit anti-WEE1 antibody (Abcam, Cat # ab137377; diluted 1:1000), mouse anti-p53 antibody (Santa Cruz Biotechnology, Cat # sc-126; diluted 1:1000), rabbit anti-FOXO1 antibody (Cell Signaling Technology, Cat # 2880S; diluted 1:1000), rabbit anti-Cl-PARP-1 (Cell Signaling Technology, Cat # 5625 T, diluted 1:750), rabbit anti-Vinculin (Invitrogen, Cat # 700062; diluted 1:2000), or mouse anti-GAPDH (Santa Cruz Biotechnology, Cat # sc-47724; diluted 1:10,000) for overnight incubation at 4 °C. The blots were washed three times with 1X TBST for 5 min each and then probed with a secondary antibody, donkey anti-rabbit IgG (H + L), horseradish peroxidase (HRP) (Abcam, Cat # ab7083, diluted 1:5000) or goat anti-mouse IgG (H + L) Poly-HRP (ThermoFisher, Cat # 32230, diluted 1:5000) for 1–2 h at room temperature. Following three washes with 1× TBST for 5 min each, blots were detected by chemiluminescence using a BioRad ChemiDoc™ Touch Imaging System (Biorad). Densitometry analysis of protein bands in immunoblots was performed using ImageJ software as described here: https://imagej.nih.gov/ij/docs/examples/dot-blot/. Briefly, bands in each lane were grouped as a row or a horizontal "lane" and quantified using FIJI's gel analysis function. Intensity data for the duAb bands was first normalized to band intensity of either GAPDH or Vinculin in each lane then to the average band intensity for empty duAb vector control cases across replicates.

Structure prediction

All structures were predicted via the AlphaFold3 server (https://alphafoldserver.com/), and the shading was done according to AlphaFold's confidence metric, plDDT, as follows: Very low (plDDT <50) = Orange, Low (70 > plDDT > 50) = Yellow, Confident (70 > plDDT > 90) = Light Blue, Very high (plDDT > 90) = Light Blue.

Statistical analysis and reproducibility

Sample sizes were not predetermined based on statistical methods but were chosen according to the standards of the field (three independent biological replicates for each condition), which gave sufficient statistics for the effect sizes of interest. All data were reported as average values with error bars representing standard deviation (SD). Statistical analysis was performed using the two-tailed Student's t-test using GraphPad Prism 10 software, with calculated p values are represented as follows: $^*p \le 0.05$, $^{**}p \le 0.01$, $^{***}p \le 0.001$, $^{****}p \le 0.0001$. The p value representations above each bar in the fold stabilization and densitometry analyses are indicative of comparisons between the control and the respective sample; all other p value notations are between the specified samples. No data were excluded from the analyses. The experiments were not randomized. The investigators were not blinded to allocation during experiments and outcome assessment.

Reporting summary

Further information on research design is available in the Nature Portfolio Reporting Summary linked to this article.

Data availability

All data needed to evaluate the conclusions in the paper are present in the paper and supplementary tables. Raw and processed data underlying graphical figures (including raw immunoblots) are provided as Source Data, which can be found in our Zenodo depository: https://doi.org/10.5281/zenodo.15121468. The

duAb cloning vector (#232089) has been deposited to Addgene: https://www.addgene.org/232089/. Source data are provided with this paper.

References

1. Zhao, L., Zhao, J., Zhong, K., Tong, A. & Jia, D. Targeted protein degradation: mechanisms, strategies and application. *Signal Transduct. Target. Ther.* **7**, 1–13 (2022).
2. Sabapathy, K. & Lane, D. P. Therapeutic targeting of p53: all mutants are equal, but some mutants are more equal than others. *Nat. Rev. Clin. Oncol.* **15**, 13–30 (2018).
3. Ward, C. L., Omura, S. & Kopito, R. R. Degradation of CFTR by the ubiquitin-proteasome pathway. *Cell* **83**, 121–127 (1995).
4. Rao, G., Croft, B., Teng, C. & Awasthi, V. Ubiquitin-proteasome system in neurodegenerative disorders. *J. Drug Metab. Toxicol.* **6**, 187 (2015).
5. Costes, S. et al. β-cell dysfunctional ERAD/ubiquitin/proteasome system in type 2 diabetes mediated by islet amyloid polypeptide-induced UCH-L1 deficiency. *Diabetes* **60**, 227–238 (2011).
6. Henning, N. J. et al. Deubiquitinase-targeting chimeras for targeted protein stabilization. *Nat. Chem. Biol.* **18**, 412–421 (2022).
7. Chen, T., Hong, L., Yudistyra, V., Vincoff, S. & Chatterjee, P. Generative design of therapeutics that bind and modulate protein states. *Curr. Opin. Biomed. Eng.* **28**, 100496 (2023).
8. Portnoff, A. D., Stephens, E. A., Varner, J. D. & DeLisa, M. P. Ubiquibodies, synthetic E3 ubiquitin ligases endowed with unnatural substrate specificity for targeted protein silencing. *J. Biol. Chem.* **289**, 7844–7855 (2014).
9. Chatterjee, P. et al. Targeted intracellular degradation of SARS-CoV-2 via computationally optimized peptide fusions. *Commun. Biol.* **3**, 1–8 (2020).
10. Brixi, G. et al. SaLT&PepPr is an interface-predicting language model for designing peptide-guided protein degraders. *Commun. Biol.* **6**, 1081 (2023).
11. Chen, T. et al. PepMLM: Target sequence-conditioned generation of peptide binders via masked language modeling. https://doi.org/10.48550/ARXIV.2310.03842 (2023).
12. Bhat, S. et al. De novo design of peptide binders to conformationally diverse targets with contrastive language modeling. *Sci. Adv.* https://doi.org/10.1126/sciadv.adr8638 (2025).
13. Kanner, S. A., Shuja, Z., Choudhury, P., Jain, A. & Colecraft, H. M. Targeted deubiquitination rescues distinct trafficking-deficient ion channelopathies. *Nat. Methods* **17**, 1245–1253 (2020).
14. Poirson, J. et al. Proteome-scale discovery of protein degradation and stabilization effectors. *Nature* **628**, 878–886 (2024).
15. UniProt Consortium. UniProt: the universal protein knowledgebase in 2023. *Nucleic Acids Res.* **51**, D523–D531 (2023).
16. Jespersen, T. et al. The KCNQ1 potassium channel is down-regulated by ubiquitylating enzymes of the Nedd4/Nedd4-like family. *Cardiovasc. Res.* **74**, 64–74 (2007).
17. Hsu, F.-S. et al. PR-619, a General inhibitor of deubiquitylating enzymes, diminishes cisplatin resistance in urothelial carcinoma cells through the suppression of c-Myc: an in vitro and in vivo study. *Int. J. Mol. Sci.* **22**, 11706 (2021).
18. Seo, S. U. et al. Phosphorylation of OTUB1 at Tyr 26 stabilizes the mTORC1 component, Raptor. *Cell Death Differ.* **30**, 82–93 (2023).
19. Wu, Q., Huang, Y., Gu, L., Chang, Z. & Li, G.-M. OTUB1 stabilizes mismatch repair protein MSH2 by blocking ubiquitination. *J. Biol. Chem.* **296**, 100466 (2021).
20. Tan, C. W., Gardiner, B. S., Hirokawa, Y., Smith, D. W. & Burgess, A. W. Analysis of Wnt signaling β-catenin spatial dynamics in HEK293T cells. *BMC Syst. Biol.* **8**, 44 (2014).
21. Horst, D. et al. Differential WNT activity in colorectal cancer confers limited tumorigenic potential and is regulated by MAPK signaling. *Cancer Res.* **72**, 1547–1556 (2012).
22. Moshkovsky, A. R. & Kirschner, M. W. The nonredundant nature of the Axin2 regulatory network in the canonical Wnt signaling pathway. *Proc. Natl Acad. Sci. USA* **119**, e2108408119 (2022).
23. Cao, J.-H. et al. NEIL1 drives the initiation of colorectal cancer through transcriptional regulation of COL17A1. *Cell Rep.* **43**, 113654 (2024).
24. Hori, S. FOXP3 as a master regulator of Treg cells. *Nat. Rev. Immunol.* **21**, 618–619 (2021).
25. Barbi, J., Pardoll, D. M. & Pan, F. Ubiquitin-dependent regulation of Foxp3 and Treg function. *Immunol. Rev.* **266**, 27–45 (2015).
26. Wu, Y. et al. FOXP3 controls regulatory T cell function through cooperation with NFAT. *Cell* **126**, 375–387 (2006).
27. Lozano, T. et al. Blockage of FOXP3 transcription factor dimerization and FOXP3/AML1 interaction inhibits T regulatory cell activity: sequence optimization of a peptide inhibitor. *Oncotarget* **8**, 71709–71724 (2017).
28. Ghelli Luserna di Rorà, A., Cerchione, C., Martinelli, G. & Simonetti, G. A WEE1 family business: regulation of mitosis, cancer progression, and therapeutic target. *J. Hematol. Oncol.* **13**, 126 (2020).
29. Hashimoto, O. et al. Inhibition of proteasome-dependent degradation of Wee1 in G2-arrested Hep3B cells by TGF beta 1. *Mol. Carcinog.* **36**, 171–182 (2003).
30. Cruz, L., Soares, P. & Correia, M. Ubiquitin-specific proteases: players in cancer cellular processes. *Pharmaceuticals* **14**, 848 (2021).
31. Seong, B. K. A. et al. TRIM8 modulates the EWS/FLI oncoprotein to promote survival in Ewing sarcoma. *Cancer Cell* **39**, 1262–1278.e7 (2021).
32. Tripathi, S. et al. Defining the condensate landscape of fusion oncoproteins. *Nat. Commun.* **14**, 1–25 (2023).
33. Linardic, C. M. PAX3-FOXO1 fusion gene in rhabdomyosarcoma. *Cancer Lett.* **270**, 10–18 (2008).
34. Kastenhuber, E. R. & Lowe, S. W. Putting p53 in context. *Cell* **170**, 1062–1078 (2017).
35. Lavin, M. F. & Gueven, N. The complexity of p53 stabilization and activation. *Cell Death Differ.* **13**, 941–950 (2006).
36. Wesierska-Gadek, J., Schloffer, D., Kotala, V. & Horky, M. Escape of p53 protein from E6-mediated degradation in HeLa cells after cisplatin therapy. *Int. J. Cancer* **101**, 128–136 (2002).
37. Cheng, Q. et al. Selective organ targeting (SORT) nanoparticles for tissue-specific mRNA delivery and CRISPR-Cas gene editing. *Nat. Nanotechnol.* **15**, 313–320 (2020).
38. Ghosal, S. et al. Nanoparticle-mediated delivery of peptide-based degraders enables targeted protein degradation. Preprint at *bioRxiv* https://doi.org/10.1101/2024.03.17.584721 (2024).
39. Riley, R. S. et al. Ionizable lipid nanoparticles for in utero mRNA delivery. *Sci. Adv.* **7**, eaba1028 (2021).
40. Chan, A. et al. Lipid-mediated intracellular delivery of recombinant bioPROTACs for the rapid degradation of undruggable proteins. *Nat. Commun.* **15**, 5808 (2024).
41. Ye, T. et al. Programmable protein degraders enable selective knockdown of pathogenic β-catenin subpopulations in vitro and in vivo. Preprint at *bioRxiv* https://doi.org/10.1101/2024.11.10.622803 (2024).
42. Mashimo, M. et al. The 89-kDa PARP1 cleavage fragment serves as a cytoplasmic PAR carrier to induce AIF-mediated apoptosis. *J. Biol. Chem.* **296**, 100046 (2021).
43. Knipscheer, P. et al. Ubc9 sumoylation regulates SUMO target discrimination. *Mol. Cell* **31**, 371–382 (2008).
44. Zhong, Q. et al. Protein posttranslational modifications in health and diseases: Functions, regulatory mechanisms, and therapeutic implications. *MedComm (2020)* **4**, e261 (2023).
45. Das, C. et al. Structural basis for conformational plasticity of the Parkinson's disease-associated ubiquitin hydrolase UCH-L1. *Proc. Natl Acad. Sci. USA* **103**, 4675–4680 (2006).

46. Bishop, P., Rocca, D. & Henley, J. M. Ubiquitin C-terminal hydrolase L1 (UCH-L1): structure, distribution and roles in brain function and dysfunction. *Biochem J.* **473**, 2453–2462 (2016).
47. Madiraju, C., Novack, J. P., Reed, J. C. & Matsuzawa, S.-I. K63 ubiquitination in immune signaling. *Trends Immunol.* **43**, 148–162 (2022).
48. Mevissen, T. E. T. et al. OTU deubiquitinases reveal mechanisms of linkage specificity and enable ubiquitin chain restriction analysis. *Cell* **154**, 169–184 (2013).
49. Hou, X., Zaks, T., Langer, R. & Dong, Y. Lipid nanoparticles for mRNA delivery. *Nat. Rev. Mater.* **6**, 1078–1094 (2021).
50. Chen, Y. et al. Proteolysis-targeting chimera (PROTAC) delivery system: advancing protein degraders towards clinical translation. *Chem. Soc. Rev.* **51**, 5330–5350 (2022).
51. Patel, N. et al. Development and characterization of an in vitro cell-based assay to predict potency of mRNA-LNP-based vaccines. *Vaccines* **11**, 1224 (2023).
52. Kampmann, M. CRISPRi and CRISPRa screens in mammalian cells for precision biology and medicine. *ACS Chem. Biol.* **13**, 406–416 (2018).
53. Peng, Z., Schussheim, B. & Chatterjee, P. PTM-Mamba: a PTM-aware protein language model with bidirectional gated Mamba blocks. *Nat. Methods* https://doi.org/10.1038/s41592-025-02656-9 (2025).
54. Chen, T., Zhang, Y. & Chatterjee, P. moPPIt: generation of motif-specific binders with protein language models. Preprint at *bioRxiv* https://doi.org/10.1101/2024.07.31.606098 (2024).
55. Vincoff, S. et al. FusOn-pLM: a fusion oncoprotein-specific language model via adjusted rate masking. *Nat. Commun.* **16**, 1–11 (2025).

Acknowledgements

We thank the Colecraft Lab at Columbia University for providing enDUBO1 and KCNQ1-YFP constructs. We also thank Dr. Matthew Foster and Marlene Violette at the Duke Proteomics and Metabolomics Core Facility for assistance with proteomics experiments and analysis. We further thank Dr. Qianben Wang and Dr. Zhifen Cui at Duke University for allowing usage of the NanoAssemblr Spark for lipid nanoparticle formulation and providing technical expertise. The research was supported by institutional startup funds to the lab of P.C. from Duke University, as well as the Wallace H. Coulter Foundation, The Hartwell Foundation, and NIH grants 3U54CA231630-01A1S4 and 1R21CA278468-01. The SaLT&PepPr and PepPrCLIP algorithms were provided and developed in conjunction with UbiquiTx, Inc.

Author contributions

L.H. built constructs, conducted transfections, carried out Western blotting and flow cytometry experiments, and performed data analyses, with assistance from T.Z.W., D.S., and R.W. T.Y. conducted WEE1 experiments. T.Z.W. conducted p53 LNP experiments with assistance from H.L. L.Z. developed fluorescent reporter cell lines. S.V. and T.C. designed guide peptides, with assistance from K.K. and S.G. P.C. and L.H. wrote the manuscript. All authors reviewed and edited the paper. M.P.D supervised WEE1 experiments. P.C. conceived, designed, directed, and supervised the study.

Competing interests

P.C., L.H., and M.P.D. are listed as inventors on US Patent Application 63/541,921: "Peptide-Guided Protein Stabilizers and Uses Thereof". P.C. and M.P.D. are co-founders of UbiquiTx, Inc., which commercializes genetically encoded proteome editing technologies, and are co-inventors of duAb patents. P.C.'s interests are reviewed and managed by Duke University in accordance with their conflict-of-interest policies. M.P.D.'s interests are reviewed and managed by Cornell University in accordance with their conflict-of-interest policies.

Additional information

Supplementary information The online version contains supplementary material available at https://doi.org/10.1038/s41467-025-58872-6.

Correspondence and requests for materials should be addressed to Pranam Chatterjee.

Peer review information *Nature Communications* thanks Marc Güell, Matylda Izert-Nowakowska and the other, anonymous, reviewer(s) for their contribution to the peer review of this work. A peer review file is available.